A self-stabilised walking gait for humanoid robots based on the essential model with internal states

Qiuyue Luo, Christine Chevallereau, Yongsheng Ou, Jianxin Pang, Victor De-León-Gómez, Yannick Aoustin

Received: 31 July 2022 | Revised: 12 September 2022 | Accepted: 13 October 2022

IET Cyber-Systems and Robotics

DOI: 10.1049/csy2.12071

ZHEJIANG UNIVERSITY PRESS | IET The Institution of Engineering and Technology | WILEY

ORIGINAL RESEARCH

A self-stabilised walking gait for humanoid robots based on the essential model with internal states

Qiuyue Luo[1,2] | Christine Chevallereau[3] | Yongsheng Ou[1] | Jianxin Pang[2] | Victor De-León-Gómez[4] | Yannick Aoustin[3]

[1]Shenzhen Institutes of Advanced Technology, Chinese Academy of Sciences, Shenzhen, China

[2]Research Institute of UBTech Robotics, Shenzhen, China

[3]Laboratoire des Sciences du Numerique de Nantes (LS2N), CNRS, Centrale Nantes, Nantes Université, Nantes, France

[4]FCA at the Univerdidad Autónoma de Coahuila, Torreón, México

Correspondence

Yongsheng Ou, Shenzhen Institutes of Advanced Technology, Chinese Academy of Sciences, Shenzhen 518055, China.
Email: ys.ou@siat.ac.cn

Funding information

National Natural Science Foundation of China, Grant/Award Numbers: 62063006, 62173319, U1813208; Shenzhen Fundamental Research Program, Grant/Award Number: JCYJ20200109115610172; Guangdong Basic and Applied Basic Research Foundation, Grant/Award Number: 2020B1515120054; National Key Research and Development Program of China under Grant, Grant/Award Number: 2018AAA0103001

Abstract

Walking stability is one of the key issues for humanoid robots. A self-stabilised walking gait for a full dynamic model of humanoid robots is proposed. For simplified models, that is, the linear inverted pendulum model and variable-length inverted pendulum model, self-stabilisation of walking gait can be obtained if virtual constraints are properly defined. This result is extended to the full dynamic model of humanoid robots by using an essential dynamic model, which is developed based on the zero dynamics concept. With the proposed method, a robust stable walking for a humanoid robot is achieved by adjusting the step timing and landing position of the swing foot automatically, following its intrinsic dynamic characteristics. This exempts the robot from the time-consuming high-level control approaches, especially when a full dynamic model is applied. How different walking patterns/features (i.e., the swing foot motion, the vertical centre of mass motion, the switching manifold configuration, etc.) affect the stability of the walking gait is analysed. Simulations are conducted on robots Romeo and TALOS to support the results.

KEYWORDS

dynamic stability, humanoid and bipedal locomotion, passive walking

1 | INTRODUCTION

When walking on the flat ground, human beings do not pay sustained attention to this task. It can therefore be assumed that the gait of human beings encodes a certain number of properties that ensure the natural stability of the walk (i.e. self-stabilisation). The objective of this paper is to highlight some walking characteristics leading to self-stabilisation properties and to show how it can be used for the stability of walking on a complex humanoid robot.

Kajita et al. [1] introduced a preview control based on optimization to generate walking patterns and compensate for the zero moment point (ZMP) [2] error caused by the modelling error. Faraj et al. [3] used a discrete-time Model Predictive Control (MPC) to determine future footstep locations. A simplified low-dimensional model was used to release the calculation burden. In contrast to [3], Romualdi et al. [4] considered a reduced centroidal model instead of simplified models for the MPC, which enables online step adjustment. As this paper is meant to relieve the humanoid robot from the cognitive load to ensure its balance, any approach using optimization or predictive command mentioned above is excluded.

Another major difficulty of walking is to satisfy the conditions of contact with the ground, and in particular, the

condition of non-rotation of the foot related to the ZMP. On many humanoid robots, this task is performed by a stabilizer [5] or considered as a constraint by using high-level controllers [6]. In our work, to ensure that this constraint is met, it is assumed that the foot control allows the evolution of the ZMP to be imposed. In this context, the two actuators at the ankle of the robot during the single support (SS) phase are devoted to achieving a good tracking of ZMP; thus, the robot loses two control inputs and can be viewed as an under-actuated system or point contact robot. Since McGeer built the first planar passive robot [7] with four links, a lot of passive-based control methods [8, 9] have been proposed for under-actuated robots. In human walking, the duration of the steps is not always strictly identical, and biomechanists generally refer to the phase of the step [10]. A lot of researchers [11–14] have used the stance leg angle as the phase variable for defining the remaining states instead of using time. Different from the time, the phase variable allows the robot joints to be coordinated without re-synchronizing with an external clock in presence of disturbance. The notion of virtual constraints [11] will therefore be used in this work. This approach has shown its efficiency for experimental 3D walking in [15]. Our objective here is to define physical parameters that lead to stability and not to rely on optimization or machine learning [16].

The linear inverted pendulum (LIP) is a very popular and efficient tool to design the walking of humanoid robots [17–19]. The LIP model [20] assumes that the mass of the humanoid robot is concentrated as a punctual mass in its centre of gravity at a constant altitude. This model has been used to present the notion of self-synchronization and self-stabilisation [21]. The walking algorithm proposed in [21] has been extended in [22] by taking into account the vertical oscillation of the centre of mass (CoM). It has been proven in [22] that the vertical oscillation of the CoM contributes to obtaining self-stabilisation during the walk. Given the results of simplified models, the extension of the walking algorithm considering the full dynamics of the robot is studied in this paper. Here, a zero dynamic model called the essential model proposed in [23] is used to extend these results. The advantages of this essential model are as follows: (1) it has the same dimension as the 3D LIP model but considers the full dynamics of the humanoid robots; (2) it allows the generation of periodic walking gaits that ensure that the ZMP is kept in a desired position or follows a desired path.

The overall block diagram of the walking algorithm proposed in this paper is shown in Figure 1. The main contributions of this paper are as follows: (1) A new self-stabilised walking algorithm for a full dynamic model, which exempts the robot from the time-consuming high-level control approaches; (2) walking patterns/features that affect the stability of the walking gait are compared. The paper body is structured as follows. Section 2 concerns the dynamic modelling of the gait, which is naturally a hybrid model because the different phases of the SS and double support (DS) gait must be taken into account. Section 3 includes a closed-loop model to study walking stability. A so-called essential model [23], which has the same order as the LIP model but takes into account the dynamic characteristics of the complete humanoid robot, is introduced. Section 4 presents the phase variable and the condition of transition between steps. The desired trajectories of the controlled variables (i.e. the vertical motion of the CoM, the motion of the swing foot and the upper body) are defined in Section 5. Then, the proposed walking algorithm is applied to two complete humanoid robots in Section 6. Section 7 offers our conclusions.

2 | THE HYBRID DYNAMIC MODEL

One step of the humanoid robot's walk contains two phases: the SS phase and the DS phase. This DS phase is assumed to be instantaneous. Continuous differential equations and discrete components are used to describe the motion of the robot and the transition between steps during the SS phase and the DS phase.

2.1 | The continuous phase

For a robot with n joints, the dynamic model during the SS phase can be defined as follows:

$$\boldsymbol{D}(\boldsymbol{q})\ddot{\boldsymbol{q}} + \boldsymbol{H}(\boldsymbol{q}, \dot{\boldsymbol{q}}) = \mathbf{B}\boldsymbol{\Gamma}, \tag{1}$$

where $\boldsymbol{q} \in \mathbb{R}^{n\times 1}$ denotes the generalised coordinates for a humanoid robot, $\boldsymbol{D}(\boldsymbol{q})$ is the inertia matrix, $\boldsymbol{H}(\boldsymbol{q}, \dot{\boldsymbol{q}})$ groups the centrifugal, Coriolis and gravity terms, $\boldsymbol{B}$ is the input matrix and $\boldsymbol{\Gamma}$ is the vector of torques applied by actuators at each joint. Let $\mathbf{x} = \left[\boldsymbol{q}^{\mathsf{T}}, \dot{\boldsymbol{q}}^{\mathsf{T}}\right]^{\mathsf{T}}$ represent the states of the robot, and the state-variable model can be written as

$$\dot{\mathbf{x}} = \boldsymbol{f}(\mathbf{x}) + \boldsymbol{g}(\mathbf{x})\boldsymbol{\Gamma}. \tag{2}$$

2.2 | Transition between steps

The transition between steps happens when the swing foot touches the ground, that is, at the end of the SS phase. Since the reference frame is always attached to the stance foot, and the y axis is directed towards the CoM, the joint variables need to be relabelled at each transition, that is,

$$\boldsymbol{q}^{+} = \boldsymbol{E}\boldsymbol{q}^{-}, \tag{3}$$

where the superscripts $+$ and $-$ represent the instants just after and just before the transition, and the constant matrix $\boldsymbol{E}$ defines the interchange of joint positions. When the impact between the swing foot and the ground is considered, the joint velocities change due to the reaction forces at the foot. The velocities after impact can be expressed as:

$$\dot{\boldsymbol{q}}^{+} = \boldsymbol{\Delta}(\boldsymbol{q})\dot{\boldsymbol{q}}^{-}, \tag{4}$$

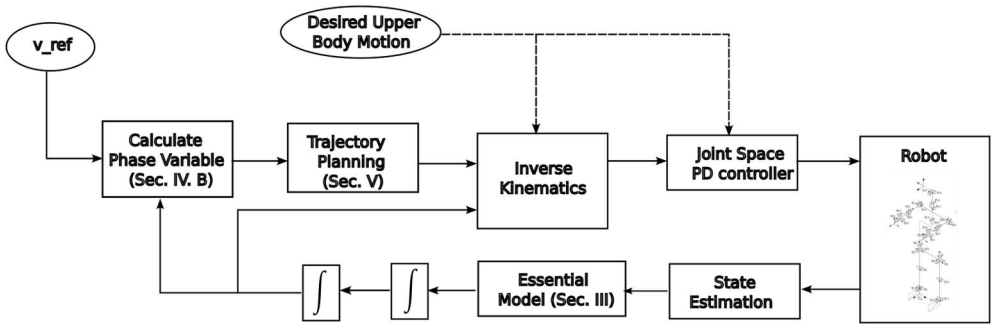

FIGURE 1 Block diagram of the proposed walking algorithm

where $\boldsymbol{\Delta}(\boldsymbol{q})$ is a matrix that relates the joint velocities after and before the impact. Note that if there is no impact at transition, $\boldsymbol{\Delta}(\boldsymbol{q}) = \boldsymbol{E}$.

2.3 | The hybrid model

At transition, the height of the swing foot is zero. Thus, a switching manifold can be defined:

$$\mathscr{S} := \{\mathbf{x} | z_s = 0\}, \tag{5}$$

where z_s represents the height of the swing foot.

By combining the continuous model Equation (2) and the transition model Equations (3) and (4), the hybrid dynamic model of the robot can be obtained:

$$\Sigma : \begin{cases} \dot{\mathbf{x}} = \boldsymbol{f}(\mathbf{x}) + \boldsymbol{g}(\mathbf{x})\boldsymbol{\Gamma}, & \mathbf{x}^- \notin \mathscr{S} \\ \mathbf{x}^+ = \boldsymbol{\Delta}_x(\mathbf{x}^-), & \mathbf{x}^- \in \mathscr{S} \end{cases} \tag{6}$$

where $\boldsymbol{\Delta}_x(\mathbf{x}^-) = \left[(\boldsymbol{E}\boldsymbol{q}^-)^\mathsf{T}, (\boldsymbol{\Delta}(\boldsymbol{q})\dot{\boldsymbol{q}}^-)^\mathsf{T}\right]^\mathsf{T}$.

3 | ZERO DYNAMICS: THE ESSENTIAL MODEL

For a fully actuated humanoid robot, the dynamic equation in the SS phase can be obtained with the Newton-Euler method:

$$\begin{bmatrix} \boldsymbol{F_0} \\ \boldsymbol{M_0} \\ \boldsymbol{\tau} \end{bmatrix} = \boldsymbol{A_e}(\boldsymbol{q})\ddot{\boldsymbol{q}} + \boldsymbol{d_e}(\boldsymbol{q}, \dot{\boldsymbol{q}}), \tag{7}$$

where $\boldsymbol{F_0} \in \mathbb{R}^{3\times 1}$ is a ground reaction force vector expressed in the world frame; $\boldsymbol{M_0} \in \mathbb{R}^{3\times 1}$ is a ground reaction moment vector expressed in the world frame; $\boldsymbol{\tau} \in \mathbb{R}^{n\times 1}$ is a torque vector generated by actuators; $\boldsymbol{A_e} \in \mathbb{R}^{(n+6)\times n}$; $\boldsymbol{d_e} \in \mathbb{R}^{(n+6)\times 1}$. The last n lines of the model correspond to Equation (1), while the first six lines give the reaction force acting on the stance foot.

For a robot with flat contact between the foot and the ground, the position of the ZMP is of primary importance. To ensure good behaviour, a stabilizer can be designed to track the desired path of the ZMP. Since the ZMP is defined via two coordinates (in sagittal and frontal directions), two inputs must be devoted to this task. Thus, only $n - 2$ other variables, denoted $\boldsymbol{q_c}$, can be controlled. Since the robot joint variables $\boldsymbol{q}$ are of dimension n, two degrees of freedom (DoFs) cannot be controlled. Here, the horizontal position of the CoM, $\boldsymbol{q_f} = [x,y]^\mathsf{T}$ is chosen as a non-controlled variable, and a model called the essential model [23] is used to define the evolution of $\boldsymbol{q_f}$ when the evolution of the ZMP and $\boldsymbol{q_c}$ is known. Furthermore, impacts of the swing foot with the ground can be considered to compute periodic walking gaits.

Perfect tracking of the reference trajectories with virtual constraints for the controlled variables $\boldsymbol{q_c}$ is assumed. The controlled joints $\boldsymbol{q_c}$ are chosen such that an homeomorphism exists between $\boldsymbol{q}$ and $[\boldsymbol{q_c}, \boldsymbol{q_f}]^\mathsf{T}$ and we can write:

$$\boldsymbol{q} = \boldsymbol{h}(\boldsymbol{q_c}, \boldsymbol{q_f}). \tag{8}$$

In this study, the controlled variables $\boldsymbol{q_c}$ are defined as functions of a phase variable denoted by Φ instead of time. The construction of the phase variable Φ is based on the non-controlled variables $\boldsymbol{q_f}$, and details will be explained in Section 4.2. In a closed loop, we have:

$$\boldsymbol{q} = \boldsymbol{h}(\boldsymbol{q_c}(\Phi(\boldsymbol{q_f})), \boldsymbol{q_f}). \tag{9}$$

The first and second time derivatives of $\boldsymbol{q}$ are:

$$\dot{\boldsymbol{q}} = \frac{\partial \boldsymbol{h}}{\partial \boldsymbol{q_c}} \frac{\partial \boldsymbol{q_c}}{\partial \Phi} \frac{\partial \Phi}{\partial \boldsymbol{q_f}} \dot{\boldsymbol{q}}_f + \frac{\partial \boldsymbol{h}}{\partial \boldsymbol{q_f}} \dot{\boldsymbol{q}}_f = \boldsymbol{J}_f \dot{\boldsymbol{q}}_f, \tag{10}$$

$$\ddot{\boldsymbol{q}} = \boldsymbol{J}_f \ddot{\boldsymbol{q}}_f + \dot{\boldsymbol{J}}_f(\boldsymbol{q}_f, \dot{\boldsymbol{q}}_f)\dot{\boldsymbol{q}}_f. \tag{11}$$

Thus, by substituting Equation (11) into Equation (7), we have:

$$\begin{bmatrix} \boldsymbol{F_0} \\ \boldsymbol{M_0} \\ \boldsymbol{\tau} \end{bmatrix} = \boldsymbol{A_e}\boldsymbol{J}_f \ddot{\boldsymbol{q}}_f + \boldsymbol{A_e}\dot{\boldsymbol{J}}_f \dot{\boldsymbol{q}}_f + \boldsymbol{d_e}(\boldsymbol{q}_f, \dot{\boldsymbol{q}}_f). \tag{12}$$

The equilibrium given by the definition of the ZMP must be satisfied for the desired ZMP positions $p_{x,d}$ and $p_{y,d}$, that is,

$$\begin{aligned} p_{x,d}F_z + M_y &= 0, \\ p_{y,d}F_z - M_x &= 0. \end{aligned} \tag{13}$$

By taking into account of rows 3–5 of Equations (12) and (13), the essential model is computed:

$$\ddot{\boldsymbol{q}}_f = \begin{bmatrix} \ddot{x} \\ \ddot{y} \end{bmatrix} = \boldsymbol{f}_\theta\left(\boldsymbol{q}_f, \dot{\boldsymbol{q}}_f, p_{x,d}, p_{y,d}\right). \tag{14}$$

More details of the development of the essential model can be found in [23].

4 | VIRTUAL CONSTRAINTS

When constraints are imposed on a system via feedback control, we call them virtual constraints [24]. In this paper, this is realized by defining the trajectories of the controlled variables $\boldsymbol{q}_c$ as functions of the robot's internal states instead of time, that is, $\boldsymbol{q}_c = \boldsymbol{q}_c(\Phi)$. Note that a phase variable must be strictly monotonic. The phase variable Φ allows us to coordinate all the joint motions of the robot without re-synchronizing with an external clock.

4.1 | Switching manifold

When the swing foot touches the ground, the geometric condition $z_s = 0$ has to be satisfied (where z_s is the height of the swing foot). There are infinite numbers of CoM positions satisfying this condition, which are grouped in the switching configuration manifold defined by

$$\mathbb{S} = \{(x, y) | z_s(\Phi(x, y)) = 0\}. \tag{15}$$

As shown in [21] for the study on the LIP model, the shape of this switching manifold is important for stability. This result is extended to the full dynamic model of the robot in our work; thus, the switching manifold proposed in [21] is considered:

$$\mathbf{S} = \{(x, y) | (x - x^{*-}) + C(y - y^{*-}) = 0\}. \tag{16}$$

where x^{*-} and y^{*-} denote the positions of the CoM in the horizontal plane at the end of the SS phase for a periodic motion. The switching manifold $\mathbf{S}$ is defined as a vertical surface parameterised by C, represented by the grey surface in Figure 2. The influence of C on stability will be studied later. The transition occures when the CoM crosses the switching manifold. Many other sets of positions can be considered, but since stability studied here is a local property, a flat surface is a convenient choice. The choice of $\mathbf{S}$ directly affects the final CoM position for a step.

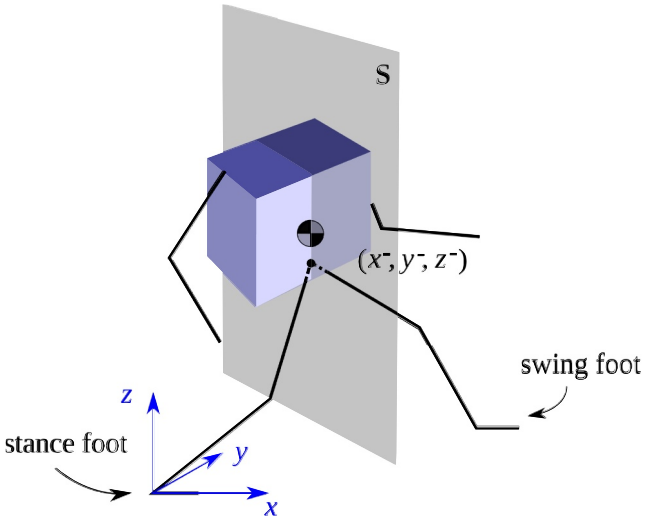

FIGURE 2 Illustration of the swing manifold **S**

The phase variable should be chosen appropriately such that the robot switches its stance leg when the CoM crosses the switching manifold.

4.2 | Phase variable

It has been proven in [21] that when the phase variable is a quadratic function of the non-controlled variables $\boldsymbol{q}_f$, self-synchronization can be obtained for the LIP model. This result is expanded in our work with the same phase variable. It will be shown that self-stabilisation can be obtained for a complete model with appropriate values of C. According to [21], the expression of the phase variable Φ is:

$$\Phi = a_1 x + a_2 y + a_3 xy + a_4 x^2 + a_5 y^2 + a_6, \tag{17}$$

where $\{a_1, a_2, a_3, a_4, a_5, a_6\}$ are the parameters that define the value of Φ. In this paper, the phase variable is supposed to vary from 0 to 1 even under the presence of perturbation. Thus, we have $\Phi(x^+, y^+) = 0$ and $\Phi(x^-, y^-) = 1$ corresponding to the beginning and end of the step. With the boundary condition defined by the switching manifold, when the lateral CoM position error is δ at the end of a step, the sagittal CoM position error should be $-C\delta$ at the end of a step. To achieve a step correctly, the condition $\Phi(x^-, y^-) = 1$ must be satisfied for any $x^- = x^{*-} - C\delta$ and $y^- = y^{*-} + \delta$; thus, four equations can be obtained:

$$\begin{cases} a_1 x^+ + a_2 y^+ + a_3 x^+ y^+ + a_4 (x^+)^2 + a_5 (y^+)^2 + a_6 = 0, \\ a_1 x^{*-} + a_2 y^{*-} + a_3 x^{*-} y^{*-} + a_4 (x^{*-})^2 + a_5 (y^{*-})^2 + a_6 = 1, \\ -a_3 C + a_4 C^2 + a_5 = 0, \\ -a_1 C + a_2 - a_3 C y^{*-} + a_3 x^{*-} - 2a_4 C x^{*-} + 2a_5 y^{*-} = 0. \end{cases} \tag{18}$$

As there are only four equations, the values $\{a_1, a_2, a_5, a_6\}$ can be calculated as functions of the two terms, namely, a_3 and a_4. The values of the a_3 and a_4 can be chosen by optimization to minimise the difference between $\Phi(x, y)$ and t/T^* in order to guarantee the monotonicity of Φ, where T^* is the desired step duration for a periodic motion. The objective function for the optimization tools is defined as

$$J = \Sigma(\Phi(x_i, y_i) - t_i/T^*)^2. \tag{19}$$

The criterion J is essentially sensitive to the step length and width. Since the optimization of (19) is not an objective of the proposed walking algorithm, and only monotonicity of the phase variable is required, the optimization is done only once unless the desired step length and width are changed.

5 | TRAJECTORIES OF THE CONTROLLED VARIABLES

The CoM height and motions of the swing foot and the upper body are defined by the desired controlled coordinates $\boldsymbol{q}_c^d(\Phi(\boldsymbol{q}_f))$. The virtual constraints are firstly expressed as outputs of the model Equation (2), that is,

$$\boldsymbol{y_{out}} := \boldsymbol{q_c} - \boldsymbol{q_c^d}(\Phi(\boldsymbol{q_f})). \tag{20}$$

Since the essential model is developed under the assumption that the reference trajectories are followed all the time, that is, the outputs of the system are identically zero:

$$\boldsymbol{y_{out}} \equiv 0; \quad \dot{\boldsymbol{y}}_{\boldsymbol{out}} \equiv 0; \quad \ddot{\boldsymbol{y}}_{\boldsymbol{out}} \equiv 0. \tag{21}$$

Achievable desired trajectories for $\boldsymbol{q}_c^d(\Phi)$ must be designed properly so that they can be tracked precisely by any well-suited control law. Therefore, the changes of velocities of the controlled variables due to impact (if they exist) must be taken into account.

The motion of the swing foot can be split into two parts: the vertical motion and the horizontal motion. The design of the vertical trajectory is based on the goal of producing an impact of the landing foot with the ground or not. For the horizontal motion, the landing place to step the foot is an important issue on which the performance of the walking gait will largely depend.

On the other hand, several research works, as in [25, 26], have proven that the motions of the trunk and arms help to improve walking efficiency. Depending on the complexity of the task, the desired upper-body motion trajectories can be defined by simple polynomials or more complex functions.

5.1 | Vertical motion of CoM

The desired vertical motion of the CoM is defined by using a 5^{th}-order polynomial function with the following boundary conditions:

$$\begin{aligned} &z_c^d(\Phi_0) = z_0, \quad &&z_c^d(\Phi_m) = z_0 + \alpha_z, \quad &&z_c^d(\Phi_f) = z_0; \\ &\dot{z}_c^d(\Phi_0) = \dot{q}_{c,1}^+, \quad &&\dot{z}_c^d(\Phi_m) = 0, \quad &&\dot{z}_c^d(\Phi_f) = v_m, \end{aligned} \tag{22}$$

where $\dot{q}_{c,1}^+$ is the vertical velocity of the CoM after the transition of stance foot,[1] $\Phi_0 = 0$ and $\Phi_f = 1$ are the desired initial and final values of Φ during a step, respectively, and $\Phi_0 < \Phi_m < \Phi_f$ is an intermediate value, which in this paper is chosen as $\Phi_m = 0.6$. The values of z_0, α_z, and v_m will be given for each different case in the following sections.

5.2 | Desired motion of the swing foot

It is desired that the swing foot lands on the ground with a zero velocity or a negative velocity. When the vertical velocity of the swing foot at landing is negative, the contact with the ground is ensured when the ground is not flat, and an impact is produced. A 5^{th}-order polynomial function is used to define the vertical evolution of the swing foot by satisfying the following boundary conditions:

$$\begin{aligned} &z_s^d(\Phi_0) = 0, \quad &&z_s^d(\Phi_m) = h_s, \quad &&z_s^d(\Phi_f) = 0; \\ &\dot{z}_s^d(\Phi_0) = \dot{q}_{c,4}^+, \quad &&\dot{z}_s^d(\Phi_m) = 0, \quad &&\dot{z}_s^d(\Phi_f) = v_s, \end{aligned} \tag{23}$$

where $\dot{q}_{c,4}^+$ is the vertical velocity of the swing foot after the transition. The values of h_s and v_s will be given for each different case in the following sections.

For the motion of the swing foot along the sagittal axis, 3^{rd}-order polynomials are used with following boundary conditions:

$$\begin{aligned} &x_s^d(\Phi_0) = x_{s0}, \quad &&x_s^d(\Phi_f) = x_{sf}, \\ &\dot{x}_s^d(\Phi_0) = \dot{q}_{c,2}^+, \quad &&\dot{x}_s^d(\Phi_f) = 0; \end{aligned} \tag{24}$$

where $\dot{q}_{c,2}^+$ is the velocity of the swing foot after transition along the sagittal axis. The motion of the swing foot along the frontal axis is similar to that along the sagittal axis. Here, the desired landing positions of the swing foot along sagittal and frontal axes are defined by

$$x_{sf} = (1 - k_S)(x^- - x^{*+}) + k_S S, \tag{25}$$

$$y_{sf} = (1 - k_D)(y^- + y^{*+}) + k_D D. \tag{26}$$

to have a general expression of the expected landing position of the swing foot. The notions S and D are the step length and width, and k_S, k_D are two parameters that adjust the landing position. The case $k_S = k_D = 0$ allows to nullify the initial CoM position error at the beginning of the next step, while the case $k_S = k_D = 1$ corresponds to the fixed step length and width. The middle values $0 < k_S < 1$ and $0 < k_D < 1$ allow the landing position to move between the two locations mentioned above. The swing foot orientation is kept constant and parallel to the ground all the time.

[1] $\dot{q}_{c,i}^+$ is the i-element of the time derivative of q_c after impact

5.3 | The upper-body motion

For the desired trajectories of the controlled variables for the upper body $q^d_{c,i}$ with $i = 8, \ldots, 29$, 3^{rd}-order polynomial functions are used with the following boundary conditions:

$$\begin{aligned} q^d_{c,i}(\Phi_0) &= k_i, \quad q^d_{c,i}(\Phi_f) = k_i, \\ \dot{q}^d_{c,i}(\Phi_0) &= \dot{q}^+_{c,i}, \quad \dot{q}^d_{c,i}(\Phi_f) = 0, \end{aligned} \tag{27}$$

where $\dot{q}^+_{c,i}$ is the velocity after transition, and k_i is the desired joint position of the i^{th} controlled variable.

6 | APPLICATION TO THE COMPLETE MODEL BASED ON THE ESSENTIAL MODEL

The essential model is exploited to take into account the characteristics on the humanoid robots Romeo [27] and TALOS [28]. Romeo has a weight of 40.8 kg, a height of 1.46 m, and 31 DoFs (6 DoFs for each leg, 1 DoF for the torso, 7 DoFs for each arm and 4 DoFs for the neck and head). Talos has a weight of 95 kg, a height of 1.75 m and 1 less DoF than Romeo at the trunk. The position and orientation of the swing foot, the height of the CoM and the upper-body motions, are considered to be the controlled variables for both robots.

6.1 | Stability analysis

The stability analysis of the proposed walking gait is performed based on the stability of the Poincaré return map [11]. A walking gait is stable when all the norms of the eigenvalues of the Jacobian matrix of the Poincaré return map are strictly less than one. Since x^- and y^- are coupled via the switching manifold **S**, the Jacobian matrix of the Poincaré return map at the fixed point and its eigenvalues are numerically calculated in the coordinate system $[x, \dot{x}, \dot{y}]$. Since it has been proven in [11] that the stability properties of orbits of the hybrid restriction dynamics carry over to the full-dimensional dynamics, only the stability of the uncontrolled variables is studied, and the essential model is sufficient to analyse the stability of the walking gaits.

How different parameters (i.e., the swing foot motion, the vertical CoM motion, the switching manifold configuration, the upper-body motion, etc.) affect the stability of the walking gait that considers the full dynamics of the robot is discussed. Besides, how different walking postures and sizes of robots affect the stability of the walking gait is also discussed.

In this section, comparisons will be done for five different cases: (1) with different landing positions defined by k_S and k_D, (2) with a constant height and a varying height of the CoM, (3) with and without swing of arms and torso, (4) with a constant ZMP and with a varying ZMP, and (5) for two different robot prototypes Romeo and TALOS. The results of stability are dependent on the choice of the switching manifold characterised by the parameter C, and the duration T of the SS phase of the periodic motion is also a key parameter. Thus, in the following cases, the eigenvalues are expressed with contours as functions of C and T.

6.2 | Influences of different landing positions on the stability

How the values of k_S and k_D as well as C and T affect the stability of the proposed walking gait based on the essential model is discussed here. Eigenvalues are calculated numerically as functions of C and T for four different cases: (1) $k_S = k_D = 0$; (2) $k_S = 1$, $k_D = 0$; (3) $k_S = 0$, $k_D = 1$; (4) $k_S = k_D = 1$. For all the cases, the robot Romeo is considered and it is supposed to have a constant height of the CoM $z_0 = 0.65$ m, no impact with the ground and a fixed upper-body motion. The position of the ZMP is supposed to be constant and kept at [0; 0]. The step length and width are $S = 0.3$ m and $D = 0.15$ m, respectively. The case with $k_S = k_D = 0$ is also used as a reference case in further studies on the influence of other parameters.

It can be seen from Figure 3 that when at least one of k_S and k_D equals to zero, there exist some sets of parameters C and T such that all the eigenvalues are smaller than one, and thus, the walk is stable. However, it is unstable for any C and T when the step length and width are fixed ($k_S = k_D = 1$) with a constant height of the CoM, because all the eigenvalues are larger than one as shown in Figure 3d. When the initial CoM position error at the beginning of a step is nullified ($k_S = k_D = 0$), a larger stability region can be observed. For the case with a fixed step length but nullified initial lateral CoM position error ($k_S = 1$, $k_D = 0$), stability can be obtained when the value of C is small, while for the case with a fixed step width but nullified initial sagittal CoM position error ($k_S = 0$, $k_D = 1$), no stability can be obtained for slow walking velocity with a step timing bigger than 0.7 s.

6.3 | Influence of the vertical CoM motion

As observed in human walking, the CoM of human beings is not constant during a step [29]. It has been proven in [22] that the vertical CoM velocity v_m being negative at transition is crucial for obtaining stability for an inverted pendulum when no high-level control is performed. How the vertical CoM motion affects walking stability of the robot Romeo is analysed here. Two cases with the same magnitude $\alpha = 0.03$ m of CoM height but different v_m (−0.1 m/s and −0.2 m/s, respectively) are considered for comparison with the reference case with a constant CoM height. The CoM height for the reference case is 0.65 m, while the mean CoM height for the comparison case is 0.65 m as well to avoid being out of the workspace. All the reference and comparison cases are supposed to have the same swing foot motion and upper-body motion with $S = 0.3$ m, $D = 0.15$ m, $k_S = k_D = 0$, $[p_x; p_y] = [0; 0]$.

It can be seen from Figure 4 that the norms of the eigenvalues are smaller for walking gaits with a larger amplitude of v_m. Stability cannot be obtained for slow walking velocities with step timing larger than 0.8 s when $v_m = -0.2$ m/s. The vertical velocity of the CoM being negative is not a necessary condition for the essential model to obtain stability, because the asymmetries in the system during the gaits due to the repartition of masses are enough to generate stability [30]. The vertical velocity of CoM being negative enlarges the stability area, especially for small values of C and reduces the norms of the eigenvalues.

6.4 | Influence of the upper-body motion

As observed in human walking, human beings swing their arms during a step to reduce the total angular momentum of the

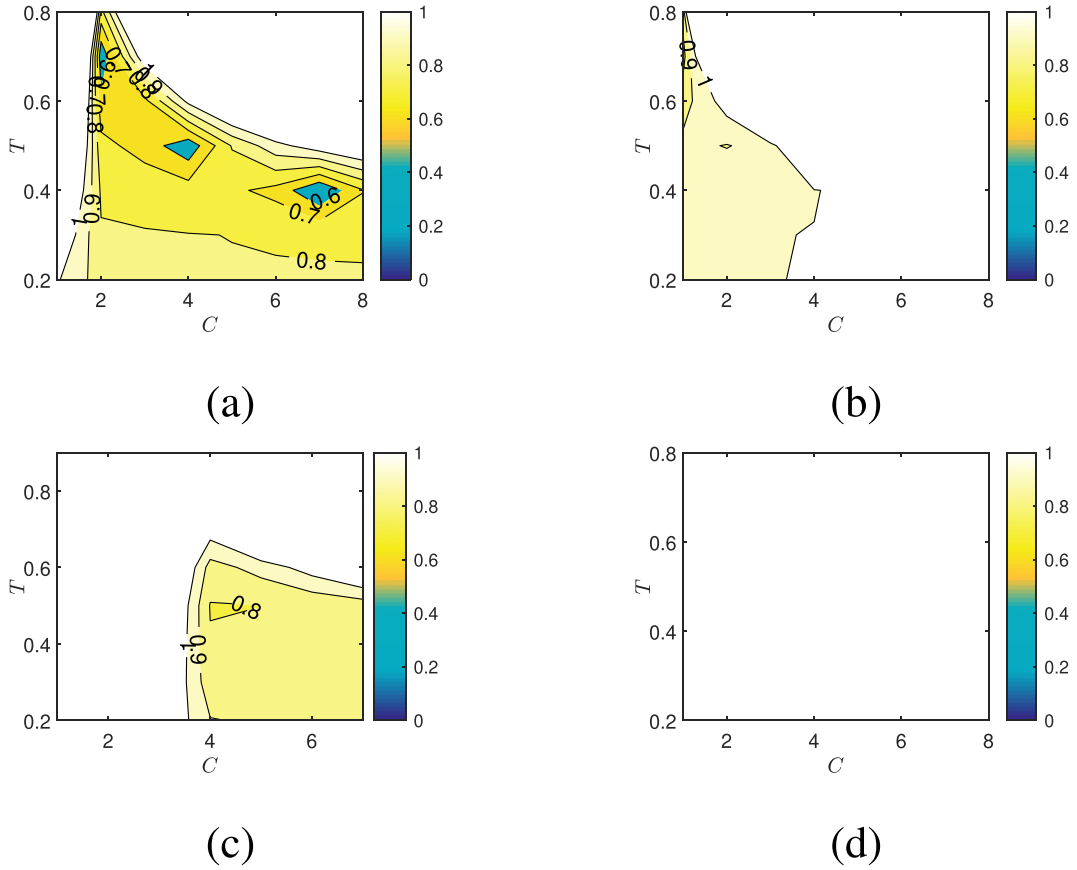

FIGURE 3 Influence of k_S and k_D on the eigenvalues for robot Romeo. Contrary to the white areas, the coloured areas indicate the self-stabilisation condition. (a) $k_S = k_D = 0$. (b) $k_S = 1$, $k_D = 0$. (c) $k_S = 0$, $k_D = 1$. (d) $k_S = k_D = 1$.

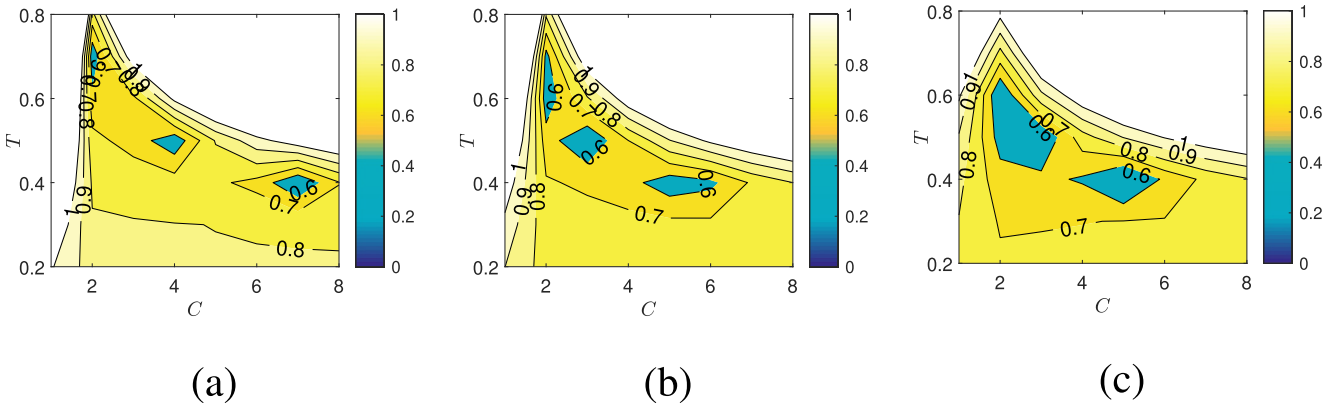

FIGURE 4 Comparison of maximum norms of eigenvalues for different v_m for robot Romeo. Contrary to the white areas, the coloured areas indicate the self-stabilisation condition. (a) $v_m = 0$. (b) $v_m = -0.1$ m/s. (c) $v_m = -0.2$ m/s.

body by creating an angular momentum in the direction opposing lower limb rotation. How this motion affects the stability of the walk is studied here. Two cases with and without the upper-body motion, that is, arm and torso swing are compared for robot Romeo here. For the case with the upper-body motion, the motions of the torso, shoulders, and elbows are shown in Table 1. Both cases are supposed to have no impact and constant CoM height with $S = 0.3$ m, $D = 0.15$ m, $k_S = 0$, $k_D = 0$, $v_s = 0$, $z_m = 0.65$ m and $[p_x; p_y] = [0; 0]$.

It can be seen from Figure 5 that the result obtained for the motion with arm and torso swings is almost the same as that obtained with a fixed upper-body motion. Although it is believed that the upper-body swing helps reduce the energy cost [31], the contribution of the upper-body swing to the stability is not as obvious with the walking algorithm proposed in this work. On the other hand, this conclusion is interesting since it shows that the stability condition obtained for one fixed upper-body motion can be used for the case with a different upper-body motion.

6.5 | Influence of ZMP evolution

One main advantage of the proposed essential model is that a desired location or a path can be imposed for the ZMP during a whole step. This section studies the influence of the ZMP evolution on the stability of walking gaits. Two cases with a constant ZMP and a varying ZMP are compared. For the case with a constant ZMP, the ZMP is constrained at the zero position, that is, $[p_{x0}; p_{y0}] = [0; 0]$ and $[p_{xf}; p_{yf}] = [0; 0]$. For the case with a varying ZMP, 3^{rd}-order polynomial functions are applied with $[p_{x0}; p_{y0}] = [-0.01; 0.02]$ m and $[p_{xf}; p_{yf}] = [0.08; 0.02]$ m. Both cases are supposed to have no impact, constant CoM height and fixed upper-body motion, with $S = 0.3$ m, $D = 0.15$ m, $k_S = 0$, $k_D = 0$, $v_s = 0$ and $z_m = 0.65$ m.

It is shown in Figure 6 that a varying ZMP enlarges the area of stability in general. However, for slow motions with $T > 0.65$ s, the maximum norm of the eigenvalues of the case with a varying ZMP is larger than that of the case with a constant ZMP.

TABLE 1 Upper-body parameters for Romeo (Unit: rad)

Description	Label	$k_{0,i}$	$k_{f,i}$
Torso yaw	$q^d_{c,10}$	0.1757	−0.1757
R. shoulder yaw	$q^d_{c,15}$	−0.3	0.2
R. elbow pitch	$q^d_{c,18}$	−0.3491	−0.7854
L. shoulder yaw	$q^d_{c,22}$	−0.2	0.3
L. elbow pitch	$q^d_{c,25}$	−0.7854	−0.3491

6.6 | Comparison of Romeo and TALOS

Romeo and TALOS are two humanoid robots with different heights, weights, and inertias. It is interesting to validate the stability of the proposed walking algorithm on different robots. The CoM heights of Romeo and TALOS are 0.7008 and 0.9424 m, respectively, when their legs are straightened. During walking, the CoM height of Romeo is chosen to be 0.65 m and that of TALOS is 0.8 m to avoid being out of workspace. With the larger size, the step length and width of TALOS are 0.4 and 0.2 m, respectively, while those of Romeo are 0.3 and 0.15 m. In this comparison, both robots are supposed to have a constant CoM height, no impact between the swing foot and the ground, and a fixed upper-body motion. The position of the ZMP is supposed to be constant and kept at the position [0; 0]. The positions of the swing feet for the two robots are chosen to nullify the initial CoM position error, that is, $k_S = k_D = 0$.

It can be seen from Figure 7 that the stability area for TALOS is slightly larger than that for Romeo. When the step duration increases, the range of proper values of C decreases for both robots. In conclusion, a similar choice of C and T can be used for the two robots.

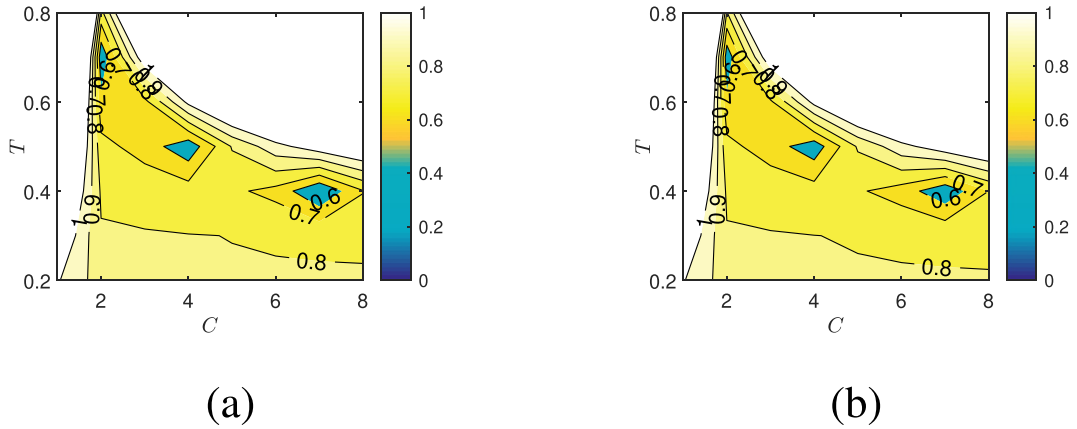

FIGURE 5 Comparison of maximum norms of eigenvalues for different upper-body motions for robot Romeo. Contrary to the white areas, the coloured areas indicate the self-stabilisation condition. (a) Fixed upper-body motion. (b) Motion with arm and torso swings.

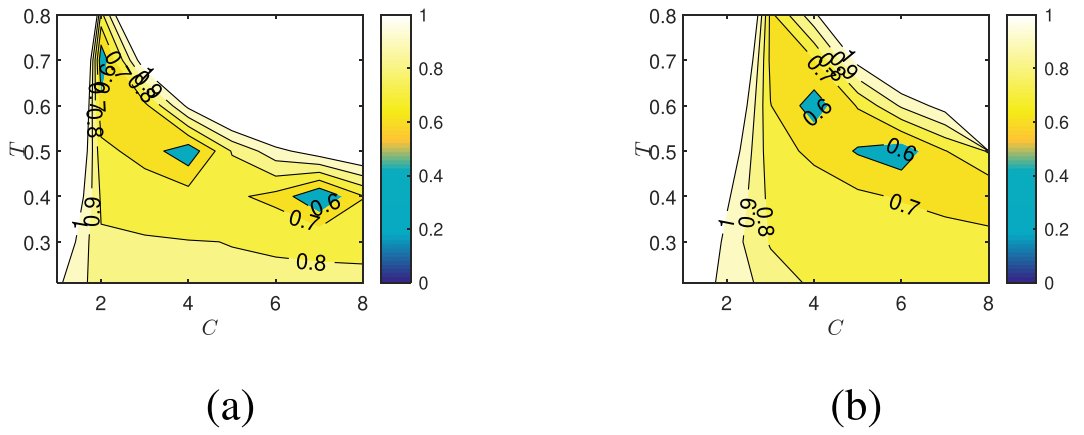

FIGURE 6 Comparison of maximum norms of eigenvalues for different zero moment point (ZMP) evolutions for robot Romeo. Contrary to the white areas, the coloured areas indicate the self-stabilisation condition. (a) Motion with a constant ZMP. (b) Motion with a varying ZMP.

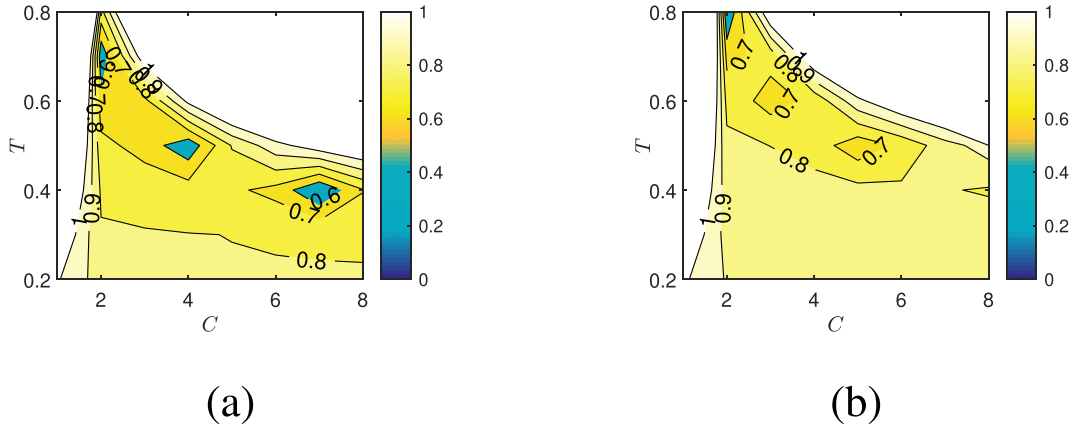

FIGURE 7 Comparison of maximum norms of eigenvalues for Romeo and TALOS. Contrary to the white areas, the coloured areas indicate the self-stabilisation condition. (a) Romeo and (b) TALOS.

6.7 | Simulations

By considering the stability conditions discussed in the previous section, simulations will be performed for robots Romeo and TALOS in this section. The starting phase strategy used in [22] is applied here. Since the motion at the starting phase does not affect the stability of walking during the periodic motion, the starting phase strategy will not be discussed here.

6.8 | Change of step width

In this section, a human-like walking pattern is considered for robot Romeo, that is, with a varying CoM height and swing of arms and torso. The parameters of the CoM and swing foot motions are shown in Table 2. Except for the first step, the position of the ZMP is expected to follow a 3^{rd}-order polynomial function varying from $[p_{x0}; p_{y0}] = [-0.01; 0.02]$ m to $[p_{xf}; p_{yf}] = [0.08; 0.02]$ m, and the step timing for the periodic motion is expected to be 0.7 s. A change of step width from $D_1 = 0.15$ m to $D_2 = 0.2$ m is expected at the 15^{th} step. The step length for the periodic value remains $S = 0.3$ m. Since the proper value of switching manifold parameter C is proportional to the ratio

TABLE 2 Gait parameters for simulations of Romeo and TALOS

Parameter	Unit	Romeo	TALOS	Description
k_S	[m]	0	0	Landing position parameter along the x axis
k_D	[m]	0	0	Landing position parameter along the y axis
T	[s]	0.7	0.5	Step time
z_0	[m]	0.6	0.8	Height of the CoM
h_s	[m]	0.05	0.05	Maximum swing foot amplitude
$\varphi_{f,0}$	[deg]	0	0	Free foot initial rotation
φ_{ff}	[deg]	0	0	Free foot final rotation
α_z	[m]	0.05	0.05	Maximum CoM amplitude
v_m	[m/s]	−0.1	−0.1	Desired vertical CoM velocity at transition
v_s	[m/s]	−0.1	−0.1	Desired landing velocity
$[p_{x0}; p_{y0}]$	[m]	[−0.01; 0.02]	[0; 0]	Starting point of ZMP
$[p_{xf}; p_{yf}]$	[m]	[0.08; 0.02]	[0; 0]	Ending point of ZMP

Abbreviations: CoM, centre of mass; ZMP, zero moment point.

of $\frac{S}{D}$, when C_1 for $D_1 = 0.15$ m is chosen to be 3, the value of C_2 for $D_2 = 0.2$ m should be $C_2 = \frac{C_1 D_1}{D_2} = 2.25$. The fixed value defining the state of CoM for $D_1 = 0.15$ m is:

$$\boldsymbol{X}_{c1}^{*-} = \left[\frac{S}{2} + D_{x1},\ \frac{D_1}{2} + D_{y2},\ \dot{x}_{c1}^{*-},\ \dot{y}_{c1}^{*-}\right]^{\top}$$
$$= [0.193\ \text{m},\ 0.077\ \text{m},\ 0.544\ \text{m/s},\ 0.177\ \text{m/s}]^{\top}.$$

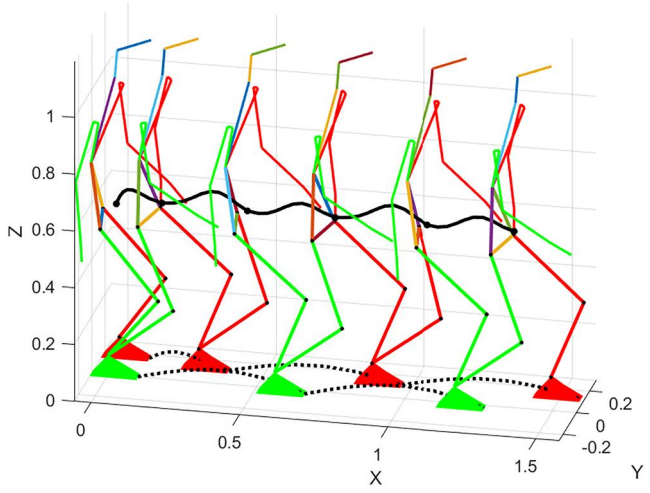

FIGURE 8 Illustration of 5 steps for Romeo

and that for $D_2 = 0.2$ m is:

$$\boldsymbol{X}_{c2}^{*-} = \left[\frac{S}{2} + D_{x2},\ \frac{D_2}{2} + D_{y2},\ \dot{x}_{c2}^{*-},\ \dot{y}_{c2}^{*-}\right]^{\top}$$
$$= [0.192\ \text{m},\ 0.102\ \text{m},\ 0.543\ \text{m/s},\ 0.257\ \text{m/s}]^{\top}.$$

The maximum eigenvalues for these two cases are:

$$\lambda_{D=0.15} = 0.726;$$
$$\lambda_{D=0.2} = 0.787.$$

The schematic illustration of the first 5 steps including the starting phase for Romeo is shown in Figure 8. Figure 9 presents the projections of the CoM motion in horizontal, sagittal and frontal planes and the position of the stance ankle for each step. Note that the local reference frame is attached to the projection of the stance ankle on the ground, the circles in Figure 9a also represent the positions of the local frame in the world frame. From Figure 9, it can be seen that the trajectory of the CoM starts from a position close to the stance foot at the starting phase and converges to the periodic motion for $D_1 = 0.15$ m after several steps. At the 15^{th} step, it can be seen clearly that the step width is increased. The change in the step width at the 15^{th} step causes an initial CoM position error at the 16^{th} step, which is regarded as a disturbance, and then the CoM converges to the periodic motion for $D_2 = 0.2$ m. The

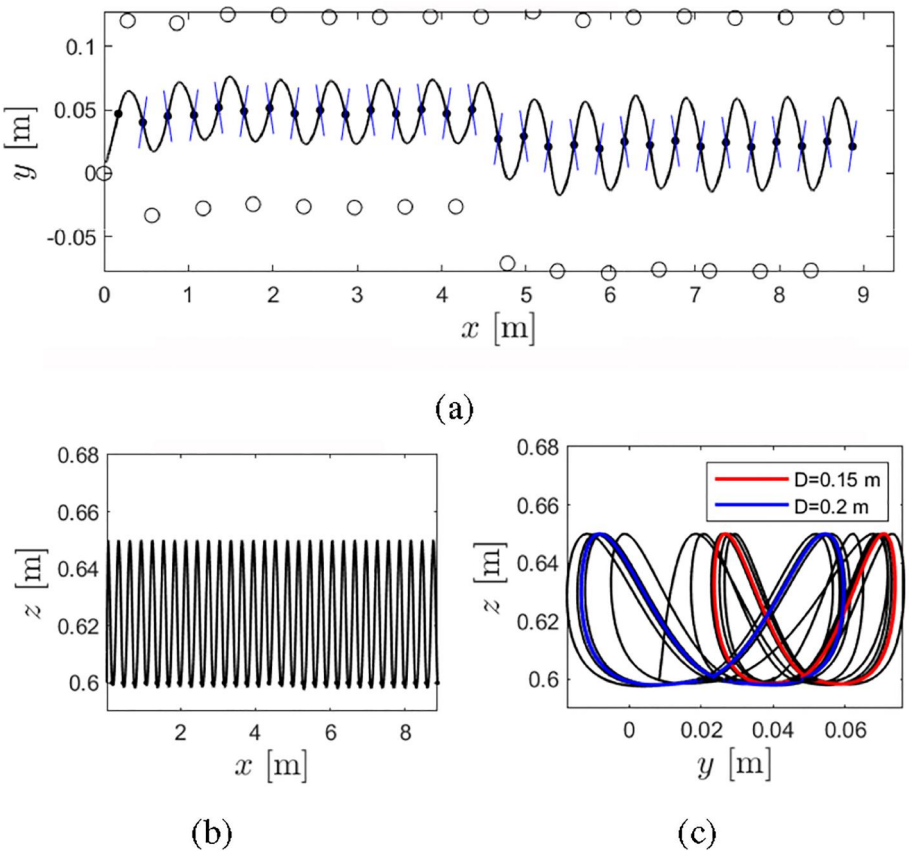

FIGURE 9 Projections of the centre of mass (CoM) trajectory in horizontal, sagittal and frontal planes. (a) Horizontal plane, the blue lines represent the switching manifold for each step, and the circles represent the positions of the zero moment point. (b) Sagittal plane. (c) Frontal plane.

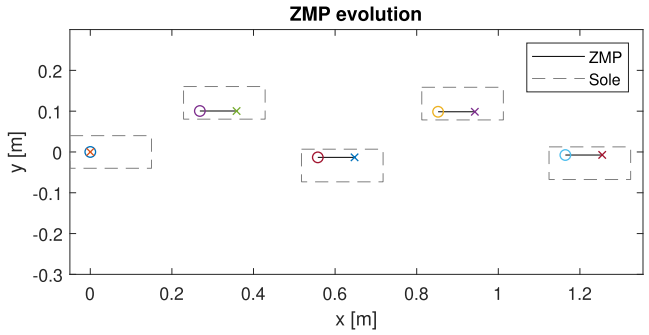

FIGURE 10 The zero moment point (ZMP) evolution of Romeo. The circles and the crosses represent the starting and ending points of the ZMP at each step.

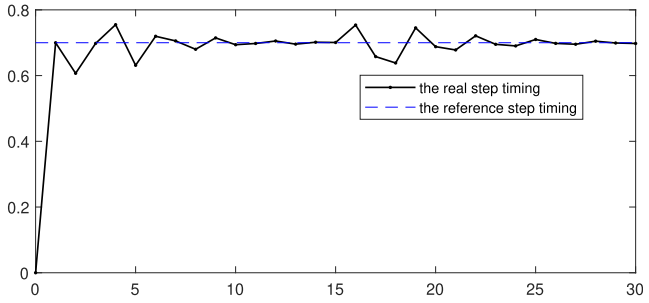

FIGURE 11 Evolution of step timing for Romeo

blue lines in Figure 9a represent the switching manifold given by (16). The cyclic motion in the frontal plane shown in Figure 9c is displaced along the y axis due to the change of D. The evolutions of the ZMP for the first 5 steps are shown in Figure 10. It can be seen that except for the starting phase, the ZMP moves from the rear to the front of the sole, following a straight segment given by the desired values. Figures 11 and 12 present the evolutions of the step timing and the state of the robot corresponding to the value of the Poincaré return map in the Poincaré section. Since the step timing is not imposed by the control law, its value varies after the starting phase and during the change of step width and eventually converges to the expected value. The variation in step timing contributes to resisting the perturbation. It can be seen that the change of step width D has a larger influence on the state along the y axis than that along the x axis. The tracking of controlled variables and the ZMP is imposed, and the free variables, that is, the horizontal position of the CoM converges to the periodic motion. Thus, self-stabilisation is obtained.

6.9 | Simulations of TALOS

In this section, another humanoid robot TALOS is analysed. A human-like walking pattern that has vertical CoM motion and swing of torso and arms with parameters shown in Table 3 is

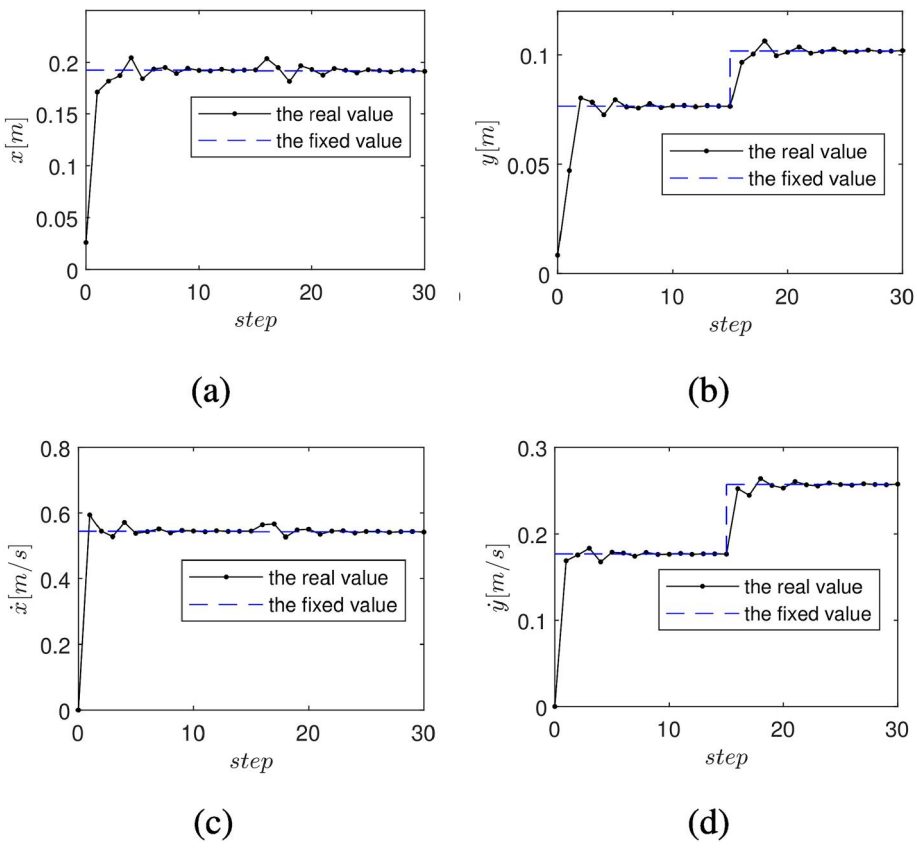

FIGURE 12 State evolution of Romeo. (a) The position of centre of mass (CoM) along the x axis. (b) The position of CoM along the y axis. (c) The velocity of CoM along the x axis. (d) The velocity of CoM along the y axis.

TABLE 3 Upper-body parameters for TALOS (Unit: rad)

Description	Label	$k_{0,i}$	$k_{f,i}$
Torso yaw	$q^d_{c,10}$	0.1757	−0.1757
R. shoulder yaw	$q^d_{c,15}$	−0.3	0.2
R. elbow pitch	$q^d_{c,18}$	−0.3491	−0.7854
L. shoulder yaw	$q^d_{c,22}$	−0.2	0.3
L. elbow pitch	$q^d_{c,25}$	−0.7854	−0.3491

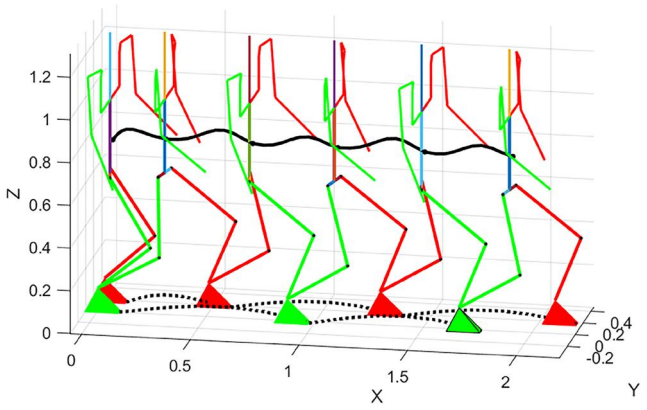

FIGURE 13 Illustration of 5 steps for TALOS

considered. The position of the ZMP is expected to be fixed at the point $\left[p^d_x; p^d_y\right] = [0; 0]$, and the step timing for the periodic motion is expected to be 0.5 s. A change of step length from $S_1 = 0.4$ m to $S_2 = 0.5$ m is expected at the 10^{th} step, while the step width remains $D = 0.2$ m. The switching manifold parameter C_1 for $S_1 = 0.4$ m is chosen to be 5 and C_2 for $S_2 = 0.5$ m is $C_2 = \frac{C_1 S_2}{S_1} = 6.25$. The fixed value defining the state of CoM for $S_1 = 0.4$ m is:

$$\begin{aligned}\boldsymbol{X}^{*-}_{c1} &= \left[x^{*-}_{c1},\ y^{*-}_{c1},\ \dot{x}^{*-}_{c1},\ \dot{y}^{*-}_{c1}\right]^\top \\ &= [0.224\ \text{m},\ 0.100\ \text{m},\ 0.933\ \text{m/s},\ 0.227\ \text{m/s}]^\top.\end{aligned}$$

and that for $S_2 = 0.5$ m is:

$$\begin{aligned}\boldsymbol{X}^{*-}_{c2} &= \left[x^{*-}_{c2},\ y^{*-}_{c2},\ \dot{x}^{*-}_{c2},\ \dot{y}^{*-}_{c2}\right]^\top \\ &= [0.278\ \text{m},\ 0.100\ \text{m},\ 1.168\ \text{m/s},\ 0.226\ \text{m/s}]^\top.\end{aligned}$$

The maximum eigenvalues for these two cases are:

$$\begin{aligned}\lambda_{S=0.4} &= 0.483; \\ \lambda_{S=0.5} &= 0.485.\end{aligned}$$

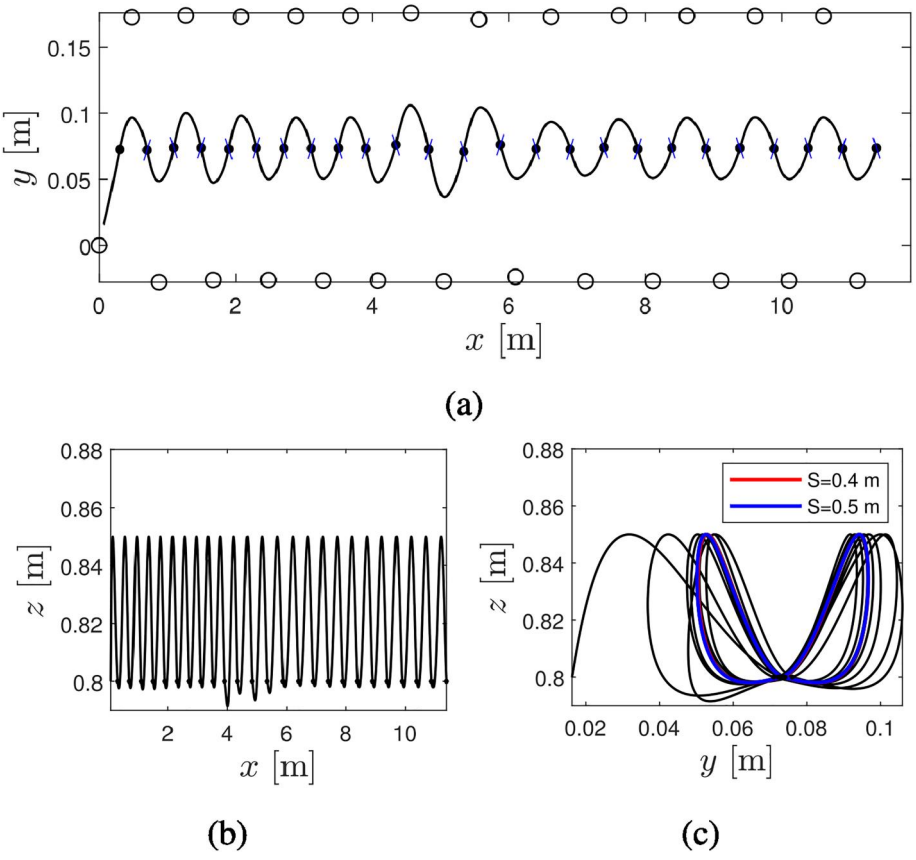

FIGURE 14 Projections of the centre of mass trajectory in horizontal, sagittal and frontal planes. (a) Horizontal plane, the blue lines represent the switching manifold for each step, and the circles represent the positions of the zero moment point. (b) Sagittal plane. (c) Frontal plane, the red curve is almost invisible because it overlaps with the blue curve.

The schematic illustration of the first 5 steps, including the starting phase, is shown in Figure 13. Figure 14 presents the projection of the CoM motion in horizontal, sagittal and frontal planes and the position of the ZMP for each step. Since the ZMP is constrained to be located at the projection of the stance leg ankle on the ground due to the condition $\left[p_x^d; p_y^d\right] = [0; 0]$, the circles in Figure 14 indicate also the stance foot locations. Figure 14 shows that the CoM converges to the periodic motions corresponding to different step lengths. The distance between the positions of two stance feet is obviously larger after the 10^{th} step due to the change of step length. In Figure 14c, the periodic motions for $S = 0.4$ m and $S = 0.5$ m overlap because the step width stays the same.

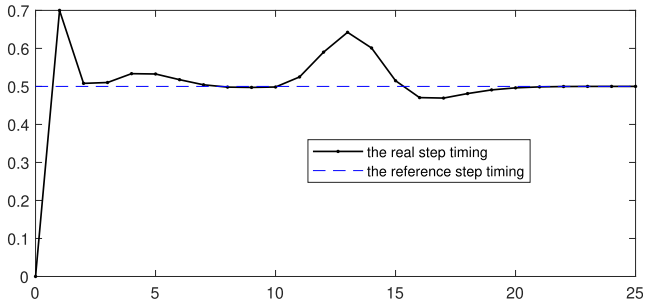

FIGURE 15 Evolution of step timing

Figures 15 and 16 present the evolution of step timing and the state of the robot, respectively. The state of the robot converges to the periodic motion during the first 10 steps and is perturbed due to the change of step length. The increase of sagittal position and velocity is obvious because the step length is increased. Meanwhile, only slight changes of the lateral position and velocity can be observed. Both the step timing and the state of the robot converge to the new expected periodic motion after the change of step length; thus, self-stabilisation is obtained.

7 | CONCLUSIONS

This paper studied the stability of periodic walking gait when the positions of the ZMP and $n - 2$ outputs (i.e. the swing foot motion, the CoM height and the upper-body motion) are controlled while the evolution of the CoM is kept free. Virtual constraints are constructed carefully to generate the motions of the controlled variables to obtain stability. A switching manifold that decides when to change the stance foot first proposed in [21] is used. By doing this, the step timing is implicitly changed under perturbation. The influence of different walking patterns/features (i.e., the swing foot motion, the vertical CoM motion, the switching manifold configuration, etc.) on the walking stability applied to the essential model is analysed. It has been shown that the upper-body motion barely affects the

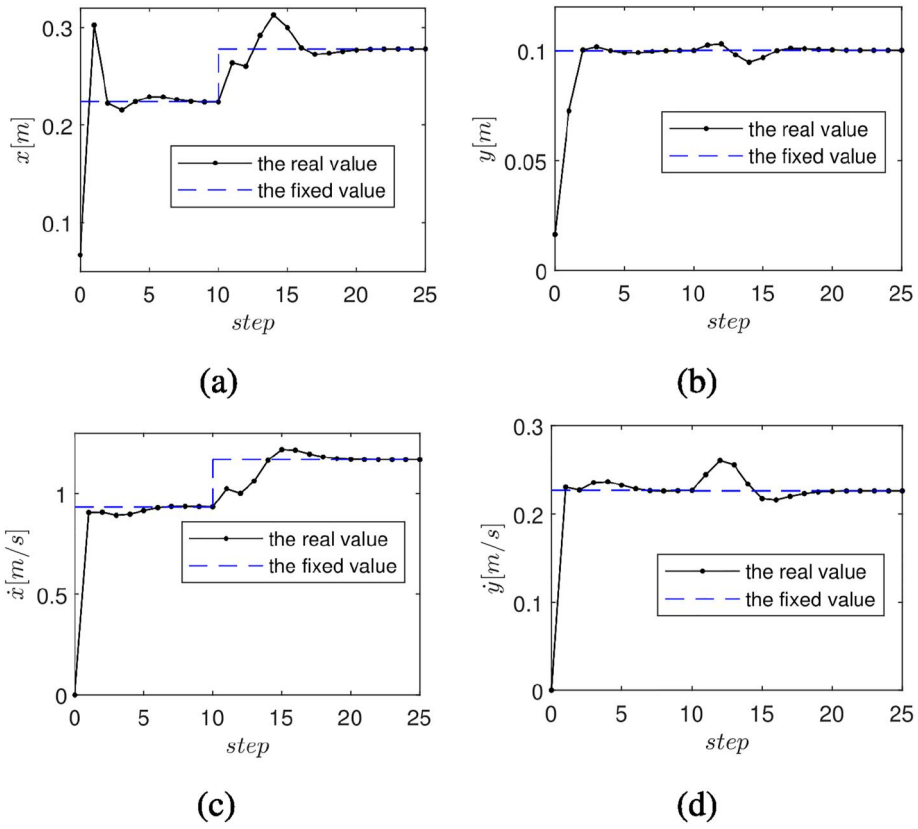

FIGURE 16 State evolution of TALOS. (a) The position of centre of mass (CoM) along the x axis. (b) The position of CoM along the y axis. (c) The velocity of CoM along the x axis. (d) The velocity of CoM along the y axis.

stability of the walking gait, while the landing position of the swing foot affects stability the most. The vertical CoM motion and ZMP evolution affect the stability slightly but not greatly. Then, simulations are carried out for robots Romeo and TALOS to validate the stability of the proposed walking algorithm on the essential model. The states of the robot converge to the desired periodic motion automatically after the change of step length or width; thus, self-stabilisation can be proven. Due to the robustness of the proposed walking algorithm, it is promising to apply this method on a real humanoid robot despite modelling errors and other disturbances. Experiments will be performed on a real robot in the future to validate this conclusion.

ACKNOWLEDGEMENTS

This work was supported by the National Key Research and Development Program of China under Grant No. 2018AAA0 103001, UBTech Robotics, National Natural Science Foundation of China (Grants No. U1813208, 62173319, and 62063006), Guangdong Basic and Applied Basic Research Foundation (No. 2020B1515120054), and Shenzhen Fundamental Research Program (No. JCYJ20200109115610172).

CONFLICT OF INTEREST

The authors declare that there is no conflict of interest that could be perceived as prejudicing the impartiality of the research reported.

DATA AVAILABILITY STATEMENT

The authors confirm that the data supporting the findings of this study are available within the article.

ORCID

Yongsheng Ou https://orcid.org/0000-0001-9653-4346

REFERENCES

1. Kajita, S., et al.: Biped walking pattern generation by using preview control of zero-moment point. In: 2003 IEEE International Conference on Robotics and Automation (Cat. No.03CH37422), vol. 2, pp. 1620–1626. (2003)
2. Vukobratovic, M., Borovac, B.: Zero-moment point-thirty five years of its life. Int. J. Humanoid Rob. 1(1), 157–173 (2004). https://doi.org/10.1142/s0219843604000083
3. Faraji, S., et al.: Versatile and robust 3d walking with a simulated humanoid robot (Atlas): a model predictive control approach. In: 2014 IEEE International Conference on Robotics and Automation (ICRA), pp. 1943–1950. (2014)
4. Romualdi, G., et al.: Online non-linear centroidal mpc for humanoid robot locomotion with step adjustment. In: 2022 International Conference on Robotics and Automation (ICRA), pp. 10412–10419. (2022)
5. Hirai, K., et al.: The development of honda humanoid robot. In: Proceedings. 1998 IEEE International Conference on Robotics and Automation (Cat. No.98CH36146), vol. 2, pp. 1321–1326. (1998)
6. Mansard, N., et al.: A versatile generalized inverted kinematics implementation for collaborative working humanoid robots: the stack of tasks. In: 2009 International Conference on Advanced Robotics, pp. 1–6. (2009)
7. McGeer, T., et al.: Passive dynamic walking. Int. J. Robot Res. 9(2), 62–82 (1990). https://doi.org/10.1177/027836499000900206
8. Asano, F., Yamakita, M., Furuta, K.: Virtual passive dynamic walking and energy-based control laws. In: 2000 IEEE/RSJ International Conference on Intelligent Robots and Systems (IROS 2000) (Cat. No.00CH37113), vol. 2, pp. 1149–1154. (2000)
9. Spong, M.W., Bullo, F.: Controlled symmetries and passive walking. IEEE Trans. Automat. Control 50(7), 1025–1031 (2005). https://doi.org/10.1109/tac.2005.851449
10. Rose, J., Gamble, J.: Human Walking, Ser. LWW Medical Book Collection. Lippincott Williams & Wilkins (2006). [Online]. https://books.google.fr/books?id=q6WrPwAACAAJ
11. Westervelt, E.R., et al.: Feedback Control of Dynamic Bipedal Robot Locomotion, vol. 28. CRC press (2007)
12. Aoustin, Y., Formal'sky, A.: Design of reference trajectory to stabilize desired nominal cyclic gait of a biped. In: Proceedings of the First Workshop on Robot Motion and Control. RoMoCo'99 (Cat. No.99EX353), pp. 159–164. (1999)
13. Freidovich, L.B., et al.: A passive 2-dof walker: hunting for gaits using virtual holonomic constraints. IEEE Trans. Robot. 25(5), 1202–1208 (2009). https://doi.org/10.1109/tro.2009.2028757
14. Chevallereau, C., Westervelt, E., Grizzle, J.: Asymptotically stable running for a five-link, four-actuator, planar bipedal robot. Int. J. Robot Res. 24(6), 431–464 (2005). https://doi.org/10.1177/0278364905054929
15. Buss, B., et al.: Experimental results for 3d bipedal robot walking based on systematic optimization of virtual constraints. In: American Control Conference, Boston, MA, USA, IEEE (2016)
16. Da, X., Grizzle, J.: Combining trajectory optimization, supervised machine learning, and model structure for mitigating the curse of dimensionality in the control of bipedal robots. IJRR 38(9), 1063–1097 (2019). https://doi.org/10.1177/0278364919859425
17. Aoustin, Y., Chevallereau, C., Laumond, J.-P.: Historical perspective of humanoid robot research in Europe. In: Humanoid Robotics: A Reference, 1–16 (2016). https://doi.org/10.1007/978-94-007-7194-9_144-1
18. Goldbeck, C., et al.: Two ways of walking: contrasting a reflexive neurocontroller and a lip-based zmp-controller on the humanoid robot armar-4. In: 2016 IEEE-RAS 16th International Conference on Humanoid Robots (Humanoids), pp. 966–972. IEEE (2016)
19. Lu, Y., et al.: Development of humanoid robot and biped walking based on linear inverted pendulum model. In: 2018 IEEE International Conference on Intelligence and Safety for Robotics (ISR), pp. 244–249. IEEE (2018)
20. Kajita, S., et al.: Biped walking pattern generator allowing auxiliary zmp control. In: 2006 IEEE/RSJ International Conference on Intelligent Robots and Systems, pp. 2993–2999. IEEE (2006)
21. Luo, Q., et al.: Self-synchronization and self-stabilization of walking gaits modeled by the three-dimensional lip model. IEEE Rob. Autom. Lett. 3(4), 3332–3339 (2018). https://doi.org/10.1109/lra.2018.2852767
22. Luo, Q., Chevallereau, C., Aoustin, Y.: Walking stability of a variable length inverted pendulum controlled with virtual constraints. Int. J. Humanoid Rob. 16(06), 1950040 (2019). [Online]. Available:. https://doi.org/10.1142/s0219843619500403
23. De-León-Gómez, V., et al.: An essential model for generating walking motions for humanoid robots. Robot. Autonom. Syst. 112, 229–243 (2019). https://doi.org/10.1016/j.robot.2018.11.015
24. Chevallereau, C., et al.: RABBIT: a testbed for advanced control theory. IEEE Control Syst. Mag. 23(5), 57–79 (2003)
25. Romkes, J., Bracht-Schweizer, K.: The effects of walking speed on upper body kinematics during gait in healthy subjects. Gait Posture 54, 304–310 (2017). https://doi.org/10.1016/j.gaitpost.2017.03.025
26. Liu, J., Schwiegelshohn, U., Urbann, O.: Stable walking of a bipedal humanoid robot involving three-dimensional upper body motion. In: 2014 IEEE-RAS International Conference on Humanoid Robots, pp. 80–85. (2014)
27. Kalouguine, A., et al.: A new human-like walking for the humanoid robot romeo. Multibody Syst. Dyn. 53(4), 411–434 (2021). https://doi.org/10.1007/s11044-021-09805-w
28. Stasse, O., et al.: Talos: a new humanoid research platform targeted for industrial applications. In: 2017 IEEE-RAS 17th International Conference on Humanoid Robotics (Humanoids), pp. 689–695. (2017)

29. Laumond, J.-P., et al.: The yoyo-man. Int. J. Robot Res. 36(13-14), 1508–1520 (2017). https://doi.org/10.1177/0278364917693292
30. Razavi, H., et al.: Symmetry in legged locomotion: a new method for designing stable periodic gaits. Aut. Robots 41(5), 1119–1142 (2017). https://doi.org/10.1007/s10514-016-9593-x
31. Aoustin, Y., Formalskii, A.: 3d walking biped: optimal swing of the arms. Multibody Syst. Dyn. 32(1), 55–66 (2014). https://doi.org/10.1007/s11044-013-9378-3

How to cite this article: Luo, Q., et al.: A self-stabilised walking gait for humanoid robots based on the essential model with internal states. IET Cyber-Syst. Robot. 1–15 (2022). https://doi.org/10.1049/csy2.12071